Optimal periodic orbits of chaotic systems occur at low period

Brian R. Hunt [1] and Edward Ott [2]
[1] *Institute for Physical Science and Technology, University of Maryland, College Park, Maryland 20742*
[2] *Institute for Plasma Research, Institute for Systems Research, and Departments of Electrical Engineering and of Physics, University of Maryland, College Park, Maryland 20742*
(Received 31 January 1996)

Invariant sets embedded in a chaotic attractor can generate time averages that differ from the average generated by typical orbits on the attractor. Motivated by two different topics (namely, controlling chaos and riddled basins of attraction), we consider the question of which invariant set yields the largest (optimal) value of an average of a given smooth function of the system state. We present numerical evidence and analysis that indicate that the optimal average is typically achieved by a low-period unstable periodic orbit embedded in the chaotic attractor. In particular, our results indicate that, if we consider that the function to be optimized depends on a parameter γ, then the Lebesgue measure in γ corresponding to optimal periodic orbits of period p or greater decreases exponentially with increasing p. Furthermore, the set of parameter values for which optimal orbits are nonperiodic typically has zero Lebesgue measure. [S1063-651X(96)10307-X]

PACS number(s): 05.45.+b

I. INTRODUCTION

Many questions concerning dynamical behavior are addressed by consideration of the long-time average of a function F of the state vector x,

$$\langle F\rangle = \lim_{t\to\infty}\frac{1}{t}\int_0^t F(x(t'))dt', \tag{1a}$$

$$\langle F\rangle = \lim_{t\to\infty}\frac{1}{t}\sum_{t'=1}^{t} F(x_{t'}), \tag{1b}$$

where t denotes time and is either continuous [Eq. (1a)] or discrete [Eq. (1b)]. [Assuming ergodicity, the time average in Eq. (1) can be replaced by a state space average over the relevant invariant measure of the system.] We call F the performance function.

In this paper we consider systems, such that, for *typical* choices of the initial x, the trajectory generated by the dynamical system is chaotic, and has a well-defined long-time average (1). (Here ''typical'' is with respect to the Lebesgue measure of initial conditions in state space.) We note, however, that atypical initial conditions may generate orbits embedded in the chaotic attractor that have different values for $\langle F\rangle$ than typical orbits. For example, consider a chaotic attractor with a basin of attraction B. Even though there is a set of initial conditions in B all yielding the *same* value for $\langle F\rangle$, and the state space volume (Lebesgue measure) of these initial conditions is equal to the entire volume of B, there is still a zero volume set of initial conditions (''atypical'' initial conditions) whose orbits asymptote to sets within the chaotic attractor but for which $\langle F\rangle$ is different from the average attained by typical orbits. A familiar case where this happens is when the initial condition is placed exactly on an unstable periodic orbit embedded in a chaotic attractor (or on the stable manifold of the unstable periodic orbit).

The question we address is the following. *Which (atypical) orbit on the attractor yields the largest value of* $\langle F\rangle$? To our knowledge this question has not been previously addressed, yet it is fundamental to at least two important problem areas of current interest:

a. Controlling chaos. In one often used method [1] for the control of chaos by use of small controls the strategy is to first identify several low-period unstable periodic orbits embedded in the chaotic attractor. One then determines the system performance that would apply if each of the various determined unstable periodic orbits were actually followed by the system. In many cases the system performance can be quantified as the value of some time average $\langle F\rangle$, as in Eq. (1). One then selects an orbit yielding performance that is best and feedback stabilizes that orbit. A question that might be asked is whether one can obtain much better performance by looking exhaustively at higher-period orbits or by considering stabilization of atypical *nonperiodic* orbits embedded in the chaotic attractor.

b. Bifurcation to riddled basins of attraction. Recently a new type of basin of attraction has been found. This new basin type is called a *riddled* basin [2,3], and has the property that any point in the basin has points in another attractor's basin arbitrarily close to it (the basin, although of positive volume, has no interior). Thus an arbitrarily small error in the determination of an initial condition may cause the orbit to go to a different attractor. This type of behavior can be present in dynamical systems that possess an invariant manifold M and a chaotic attractor in that manifold. An interesting basic question is that of how a nonriddled basin for the chaotic attractor on M becomes riddled as a system parameter is varied (i.e., the bifurcation to a riddled basin) [4]. This bifurcation occurs [5,6] when an invariant set within the strange attractor first becomes unstable for perturbations transverse to the invariant manifold M. That is, the bifurcation occurs when the transverse Lyapunov exponent maximized over all invariant sets in the chaotic attractor first becomes positive. In the simplest case, where the invariant manifold M has codimension one, the transverse Lyapunov exponent is obtained from an average of a function [as in Eq.

(1)] over the relevant orbit [5,6], and again the study of this bifurcation focuses on the invariant set maximizing an average [7].

In this paper we only treat discrete time systems (1b). The case of continuous time systems is expected to yield similar conclusions and is deferred to a future study. Our principal result is that the largest value of $\langle F \rangle$ is typically achieved by a low-period periodic orbit embedded in the chaotic attractor.

The outline of this paper is as follows. In Sec. II we consider the ''doubling transformation'' $2x$ modulo1 with a performance function $F_\gamma(x)$ with a single quadratic maximum for $x \in [0,1]$. This example reveals interesting Farey tree structure of the period of the optimal orbit as a function of the parameter γ. On the basis of this structure and other numerical results we can make several conclusions for this example. (1) The Lebesgue measure in γ corresponding to optimal periodic orbits of period p or greater decreases exponentially with p for large p. (2) The set S_γ of parameter values for which optimal orbits are nonperiodic has Lebesgue measure zero. (3) The set S_γ is uncountable, but has fractal dimension zero. (4) Optimal nonperiodic orbits for $\gamma \in S_\gamma$ are similar to periodic orbits in that they have zero topological entropy and zero fractal dimension.

In Sec. III we consider the tent map with a performance function $F(x)$ with a single quadratic maximum. We again find conclusion (1), listed above for the doubling transformation, holds. However, for the tent map we find that the parameter set S_γ, corresponding to optimal nonperiodic orbits, is empty. Thus conclusions (2)–(4) above are trivially satisfied. Furthermore, the Farey structure observed for the doubling transformation is absent, and a simpler structure prevails. We then consider several other cases in Sec. IV: the doubling transformation with a multihumped performance function, the tent map with a multihumped performance function, the Kaplan-Yorke map, and the Hénon map. It appears that in all of the examples in Sec. IV the basic structure is a combination of the two prototypical structures observed in Secs. II and III. We believe that this composite type of structure should be typical of what will occur in applications. Based on our results in Sec. IV, we conjecture that conclusions (1) and (2) above hold in general for typical low-dimensional chaotic systems and typical smooth performance functions F depending on a parameter. [For the examples of Sec. IV, we do not presently know whether S_γ is empty (as in Sec. III) or not (as in Sec. II).] Finally, we discuss the practical importance of our conclusions in the contexts of chaos control [1].

II. THE DOUBLING TRANSFORMATION WITH A SINGLE-HUMPED PERFORMANCE FUNCTION

To begin we consider a simple example, namely, the doubling transformation,

$$x_{t+1} = 2x_t \ \ (\text{modulo1}), \tag{2}$$

and for F we take

$$F_\gamma(x) = \cos[2\pi(x-\gamma)]. \tag{3}$$

Although some of the results we observe for Eqs. (2) and (3) are model specific, we claim that Eqs. (2) and (3) also yield essential behaviors that should be expected in general for low-dimensional chaotic systems. A main point will be that the optimal average is typically achieved by a low-period periodic orbit [8].

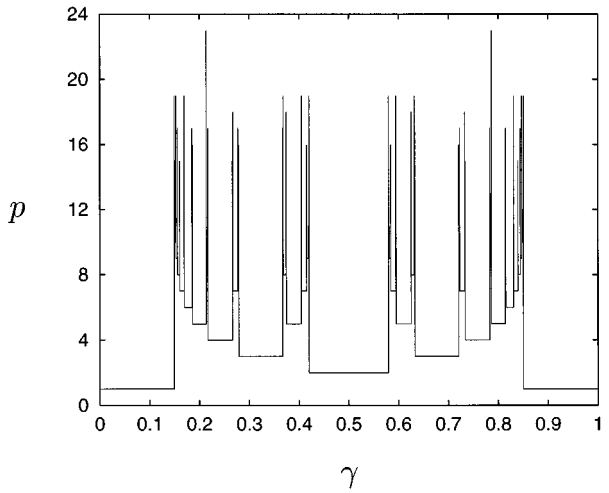

FIG. 1. Period that optimizes $\langle F_\gamma \rangle$ as a function of γ for the doubling transformation (2) and performance function (3). Unless otherwise noted, all tables and graphs are based on computations using 10^5 evenly spaced values of γ and orbits of periods 1–24.

A. Periods of optimal orbits

For each of 10^5 evenly spaced values of γ, we tested the value of $\langle F_\gamma \rangle$ for all periodic orbits of the map (2) with periods 1 to 24. There are on the order of 10^6 such orbits. Figure 1 shows the period of the orbit that maximizes $\langle F_\gamma \rangle$ for Eqs. (2) and (3) as a function of the phase angle γ. The second column of Table I gives the fraction $f(p)$ of phase values γ for which a period-p orbit maximizes $\langle F_\gamma \rangle$. For example, if γ is chosen at random in $[0,1]$, then over 93% of the time, the optimal periodic orbit does not exceed 7 in period, and more than half the time the optimal orbit's period is 1, 2, or 3. The last column in Table I gives a conjectured asymptotic prediction of the fraction $f(p)$ of the time a period-p orbit maximizes $\langle F_\gamma \rangle$ if γ is chosen at random in $[0,1]$,

$$f(p) \approx Kp2^{-p}\phi(p). \tag{4}$$

Here $\phi(p)$ is the Euler function, which is defined as the number of integers between 1 and p (inclusive) that are relatively prime to p [e.g., the numbers 1, 5, 7, and 11 are relatively prime to 12, and so $\phi(12)=4$]. Thus $\phi(p) \leqslant p-1$ for $p \geqslant 2$, and $\phi(p)=p-1$ if p is a prime. The factor K is a fitting parameter, which we choose to be 1/6 in this example. We see from Table I and the data plotted as diamonds in Fig. 2 that Eq. (4) agrees very well with the numerical results for large p [the straight line in Fig. 2 has slope $-\ln 2$ and, for the plotted diamonds, the vertical axis is the logarithm of the numerically computed $f(p)$ divided by $p\phi(p)$]. From Table I, the agreement with Eq. (4) is better than 5% for $p>5$. Note that Eq. (4) apparently has nothing to do with the precise choice of the function F_γ in Eq. (3). We believe that Eq. (4) is a good approximation for typical smooth functions

TABLE I. Numerical results for the doubling transformation (2).

	Eq. (3)		Eq. (6)		$-(x-\gamma)^2$	Eq. (4)
p	$f(p)$	$f_{90\%}(p)$	$f(p)$	$f_{90\%}(p)$	$f(p)$	$f(p)$
1	0.299	0.333	0.230	0.258	0.333	0.0833
2	0.160	0.212	0.163	0.175	0.148	0.0833
3	0.176	0.294	0.186	0.234	0.163	0.125
4	0.0985	0.143	0.0850	0.110	0.0948	0.0833
5	0.116	0.0180	0.136	0.169	0.111	0.104
6	0.0310	0	0.0350	0.0473	0.0322	0.0313
7	0.0573	0	0.0427	0.00664	0.0555	0.0547
8	0.0211	0	0.0583	0.00031	0.0210	0.0208
9	0.0178	0	0.0244	0	0.0176	0.0176
10	0.00644	0	0.00697	0	0.00652	0.00651
11	0.00918	0	0.0164	0	0.00900	0.00895
12	0.00196	0	0.00516	0	0.00196	0.00195
13	0.00324	0	0.00446	0	0.00316	0.00317
14	0.00084	0	0.00389	0	0.00086	0.00085
15	0.00062	0	0.00105	0	0.00058	0.00061
16–24	0.00092	0	0.00167	0	0.00092	0.00091

with a single maximum whose parameter dependence consists of a phase shift. Tests using other quadratic maximum, single-humped functions in place of Eq. (3) confirm this; results for $F_\gamma(x)=-(x-\gamma)^2$ are shown in the sixth column of Table I. [Although Eq. (4) appears to give a good approximation for large p, we do not know whether the relative error goes to zero as $p\to\infty$.]

Not only are low-period orbits most often optimal, but, even when a somewhat higher-period orbit is optimal, it apparently only leads to a relatively small increase in $\langle F_\gamma\rangle$ as compared to a lower-period orbit. This point is emphasized by the third column in Table I, which gives the fraction of the γ values such that the lowest-period orbit that yields a value of $\langle F_\gamma\rangle$ within 90% of the maximum value has period p. Thus, for this example, if one is willing to settle for 90% of optimal, one *never* has to go above period 5. Also for over 83% of the γ values it suffices to consider only period 1, 2, and 3. The relatively small increase of $\langle F_\gamma\rangle$ achieved by going to higher period is also evident in Fig. 3, which plots the optimal value of $\langle F_\gamma\rangle$ as a function of the phase γ. Switching of optimal periods occurs at apparent changes in the slope of this plot. For example, the inset in Fig. 3 shows $\langle F_\gamma\rangle_p$, the average of F_γ over the optimal period p orbit, versus γ for $p=3,5,8$ in the region near $\gamma\approx 0.37$. The dashed line is a weighted average of $\langle F_\gamma\rangle$ for periods 5 and 3, $(5\langle F_\gamma\rangle_5+3\langle F_\gamma\rangle_3)/(5+3)$. The optimal period 8 value of $\langle F_\gamma\rangle$ closely follows this average, but is slightly above it.

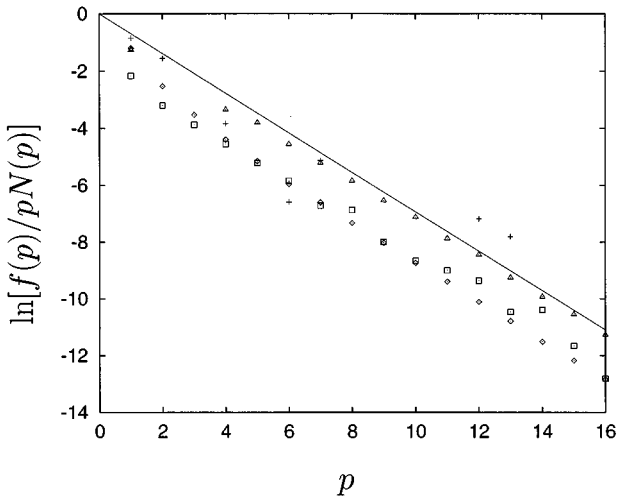

FIG. 2. Graph of $\ln[f(p)/pN(p)]$ vs p, where $N(p)$ is the number of γ intervals for which a period-p orbit is optimal. The straight line has slope $-\ln 2$. The diamonds correspond to Eqs. (2) and (3); the squares correspond to Eqs. (2) and (6), the triangles to the Kaplan-Yorke map example, and the crosses to the Hénon map example.

B. Farey tree structure

It is also interesting to note the Farey tree structure present in Fig. 1; the periods follow the pattern of the de-

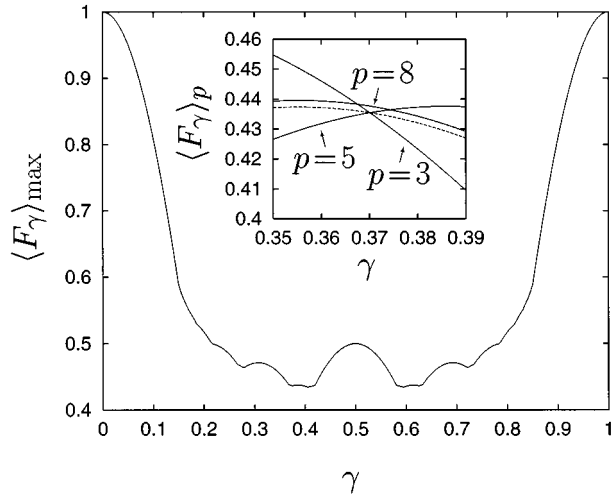

FIG. 3. Maximum value of $\langle F_\gamma\rangle$ as a function of γ for the doubling transformation (2) and function (3). Inset: closeup with added detail.

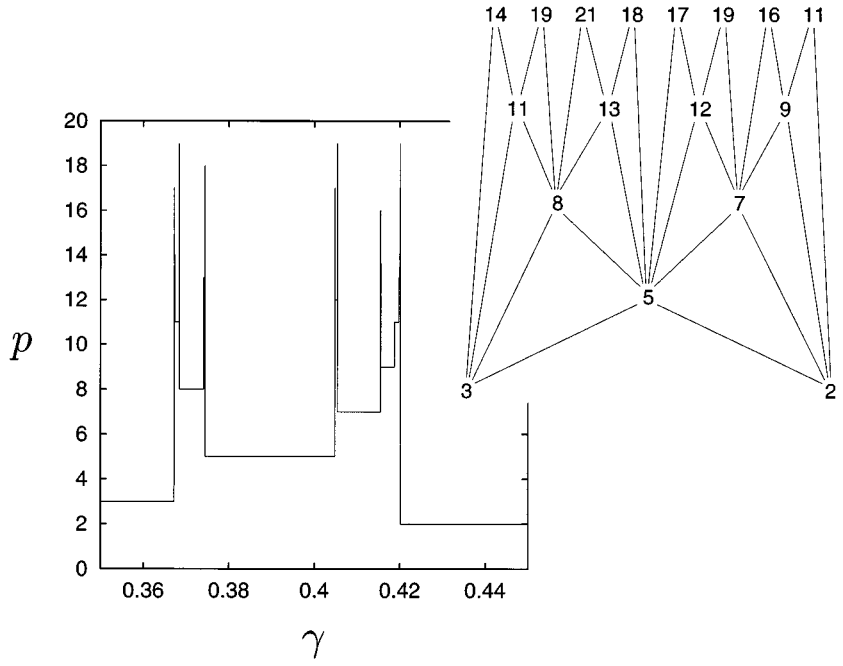

FIG. 4. Closeup of Fig. 1. Inset: the associated portion of the Farey tree.

nominators in the Farey construction of the rational numbers. That is, between any two γ intervals with optimal orbits of periods p_a and p_b and only higher periods associated with any intervening γ intervals, there is a smaller γ interval of period p_a+p_b in between, and all other γ intervals in between have period higher than p_a+p_b. This is illustrated by Fig. 1 and the magnification of the γ interval $[0.35,0.45]$ shown in Fig. 4. The inset in Fig. 4 shows the corresponding tree. Between the period-3 interval and the period-2 interval there is a period-5 interval. Between the 3 and the 5 there is an 8, between the 5 and the 2 there is a 7, and so on. Numerically we find an exponential decrease, as p increases, of the total length $r(p)=f(p)+f(p+1)+\cdots+f(p_{\max})$ of the γ intervals with period at least p (see the diamonds in Fig. 5). Noting this and thinking of optimal nonperiodic orbits as being created in the limit as the Farey tree level approaches infinity, we infer that optimal nonperiodic orbits typically do not occur on a positive Lebesgue measure set of γ.

The form of Eq. (4) is obtained as follows. The factor $\phi(p)$ is the number of times the integer p appears in the complete Farey tree (starting at the lowest level with $p_a=p_b=1$). The factor $p2^{-p}$ is obtained from our numerical observations (and by direct analytical calculation in a special case, see Appendix A) of how the width of an interval scales with the period p.

C. Fractal dimension of the set S_γ

Next, we consider the dimension of the set S_γ of γ values for which optimal orbits are nonperiodic. From the above discussion, S_γ has zero Lebesgue measure. Furthermore, S_γ can be generated by successive removal with increasing p of $\phi(p)$ intervals of optimal period p orbits from the γ interval $[0,1]$, and because of the Farey structure these intervals are separated by a positive distance from previously removed intervals. Thus S_γ is a Cantor set (in particular, S_γ is uncountable). We can determine the fractal dimension of S_γ as follows. The removal of $\phi(1)+\phi(2)+\cdots+\phi(p)$ intervals at stages 1 through p leaves of the order of p^2 unremoved intervals [recall that $\phi(p)\leqslant p-1$], which according to our numerical evidence have widths of order $p2^{-p}$ or less. Thus an ϵ covering of the unremoved intervals at stage p of the generation of S_γ requires $N(\epsilon)\sim p^2$ covering intervals if $\epsilon\sim p2^{-p}$. Noting that $[\ln N(\epsilon)]/[\ln(1/\epsilon)]\sim p^{-1}\ln(p)$ approaches zero as $p\to\infty$, we conclude that the fractal dimension of S_γ is zero.

D. Symbolic dynamics

The symbolic dynamics of the doubling transformation is particularly simple. Each orbit is represented by a sequence of two symbols, which we take to be zeros and ones, where the first symbol is 0 if the orbit is in $[0,1/2)$ and is 1 if the orbit is in $[1/2,1)$. The symbolic dynamics is then given by

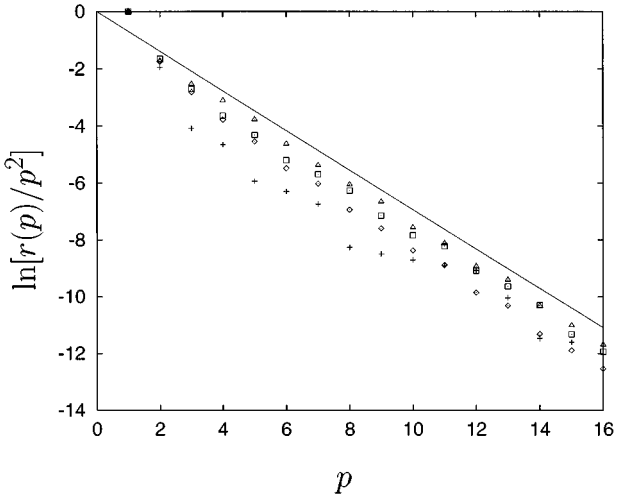

FIG. 5. Graph of $\ln[r(p)/p^2]$ vs p. The straight line has slope $-\ln 2$. The various symbols plotted correspond to the same cases as in Fig. 2.

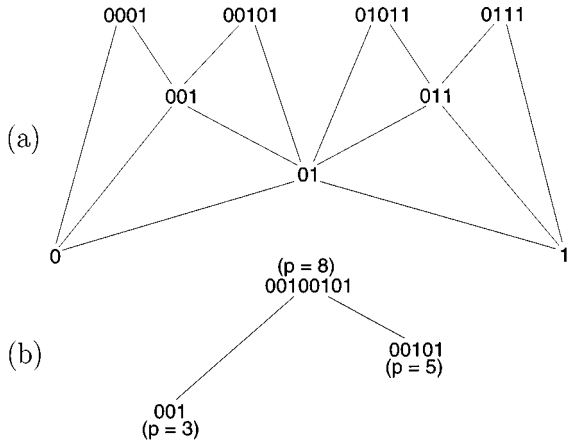

FIG. 6. (a) Farey tree specification of the symbolic dynamics of optimal periodic orbits for Eqs. (2) and (3). (b) The part of the tree in (a) corresponding to the $p=3,5,8$ periodic orbits occurring in the inset of Fig. 3.

the shift on the symbol sequences and corresponds precisely with the operation $2x$ modulo1 if x is represented in as a binary ''decimal.'' Thus each period p periodic orbit can be represented as a string of p zeros and ones (or any cyclic permutation thereof) giving the order in which the intervals $[0,1/2)$ and $[1/2,1)$ are visited. We find that the optimal periodic orbits for Eqs. (2) and (3) exhibit a very regular symbolic representation. [This structure was also found for other single-humped performance functions for which the location of the maximum was monotonic in γ, e.g., $F_\gamma(x)=-(x-\gamma)^2$.] The general scheme that we numerically observe is best expressed using the Farey tree representation shown in Fig. 6(a). Starting on the lowest tree level with the symbol 0 on the left and the symbol 1 on the right, higher levels in Fig. 6(a) are generated as follows. If there is a period p_c orbit on the tree, and its parent orbits on the tree have periods p_a and p_b, where $p_c=p_a+p_b$, then the symbol string representing the period p_c orbit is obtained by listing the p_a symbol string followed by the p_b symbol string [see Fig. 6(a)]. [Here the subscript a corresponds to the left parent orbit on the tree in Fig. 6(a), and b corresponds to the right parent orbit.]

We now consider a specific example, namely, the $p=3,5,8$ orbits occurring in the inset to Fig. 3 (see also Fig. 4). The picture obtained for this example holds for all other orbits in the Farey tree. The portion of the tree of Fig. 6(a) corresponding to these three orbits is shown in Fig. 6(b). The period-3 orbit is obtained by noting that the repeated binary expansion 0.001001001 . . . is equal to 1/7 which, using Eq. (2), gives the orbit

$$p=3:\quad \frac{1}{7}\to\frac{2}{7}\to\frac{4}{7}\to\frac{1}{7}\to\cdots.$$

Similarly, 0.001010010100101 . . . $=5/31$, and for period 5 we obtain the orbit

$$p=5:\quad \frac{5}{31}\to\frac{10}{31}\to\frac{20}{31}\to\frac{9}{31}\to\frac{18}{31}\to\frac{5}{31}\to\cdots,$$

while for period 8 we have

$$p=8:\quad \frac{37}{255}\to\frac{74}{255}\to\frac{148}{255}\to\frac{41}{255}\to\frac{82}{255}\to\frac{164}{255}\to\frac{73}{255}$$
$$\to\frac{146}{255}\to\frac{37}{255}\to\cdots.$$

We find that the period-8 orbit comes closest to the period-3 orbit at 73/255 and 2/7, respectively ($73/255-2/7\approx 2^{-11}$). For the next two iterates, the period-8 orbit closely tracks the period-3 orbit (with the distance between the two doubling on each iterate). At the third iterate of 73/255, the period-8 orbit makes its closest approach to an element of the period-5 orbit; the points involved are 74/255 and 9/31, respectively ($9/31-74/255\approx 2^{-13}$). The period-8 orbit then tracks the period-5 orbit for four more iterates, after which it again makes its closest approach to the period-3 orbit, and so on. Thus the period-8 orbit is approximated by alternately following one of its Farey parents and then the other. This explains why $\langle F_\gamma\rangle_8$ in the inset of Fig. 3 so closely follows the weighted average of $\langle F_\gamma\rangle_3$ and $\langle F_\gamma\rangle_5$ (the dashed line in the inset of Fig. 3). (A little more analysis of the placement of the various points of the periodic orbits explains why $\langle F_\gamma\rangle_8$ lies slightly above the weighted average.)

E. Metric entropy for optimal nonperiodic orbits

Next, consider a nonperiodic orbit that maximizes $\langle F_\gamma\rangle$ for some $\gamma=\gamma_0\in S_\gamma$. We claim that such an orbit has very special symbolic dynamics generated by the periodic orbits that maximize $\langle F_\gamma\rangle$ for nearby values of γ, and in fact has metric entropy zero. Recalling the Farey structure of the complement of S_γ, we regard γ_0 as being the limit of intervals in the complement of S_γ corresponding to optimal orbits of periods $p_1,p_2,\ldots$, where for $n\geqslant 3$ we have $p_n=p_a+p_b$ for some $a,b<n$. Examination of the periodic orbits that (numerically) optimize $\langle F_\gamma\rangle$ in these intervals reveals that the points in the orbit of period p_n always closely approximate the points in the orbits of periods p_a and p_b, with the approximation becoming increasingly good as n increases. We infer that the optimal nonperiodic orbit corresponding to $\gamma=\gamma_0$ is approximated arbitrarily closely by the optimal orbits of period p_n as $n\to\infty$ [9]. Furthermore, as follows from the discussion in the previous subsection, the symbolic dynamics of the optimal period p_n orbit is always a concatenation of the symbolic dynamics of the period p_a and p_b orbits that generate p_n in the Farey tree. It follows that the symbolic dynamics of the orbits of periods $p_{n+1},p_{n+2},\ldots$ are also concatenations of multiple copies of the blocks of lengths p_a and p_b corresponding to the period p_a and p_b orbits. Again we infer that the symbolic dynamics of the optimal nonperiodic orbit for $\gamma=\gamma_0$ is also composed entirely of two types of blocks of lengths p_a and p_b, concatenated in a nonperiodic fashion. It then follows that the metric entropy associated with this orbit is small; as shown in Appendix B, in a segment of N iterates along the orbit, the logarithm of the number of possible symbol sequences is at most of the order of $(N\ln p_a)/p_a$, where we assume $p_a\geqslant p_b$. Thus the entropy is at most of order $(\ln p_a)/p_a$. Since we can start this analysis arbitrarily far

TABLE II. Numerical results for the tent map (5).

	Eq. (3)		Eq. (6)		$0.234p2^{-p}$
p	$f(p)$	$f_{90\%}(p)$	$f(p)$	$f_{90\%}(p)$	$f(p)$
1	0.705	0.727	0.426	0.450	0.117
2	0.0314	0.0319	0.185	0.189	0.117
3	0.0611	0.0712	0.190	0.229	0.0878
4	0.0791	0.115	0.115	0.0791	0.0585
5	0.0580	0.0542	0.0147	0.0193	0.0366
6	0.0312	0	0.0175	0.0140	0.0219
7	0.0159	0	0.00666	0.00601	0.0128
8	0.00832	0	0.00568	0.0137	0.00731
9	0.00442	0	0.0171	0	0.00411
10	0.00238	0	0.0100	0	0.00229
11	0.00129	0	0.00540	0	0.00126
12	0.00069	0	0.00311	0	0.00068
13	0.00038	0	0.00156	0	0.00037
14	0.00020	0	0.00083	0	0.00020
15	0.00010	0	0.00048	0	0.00011
16–24	0.00012	0	0.00084	0	0.00012

along the Farey tree, p_a can be arbitrarily large, and we conclude that all optimal nonperiodic orbits have metric entropy zero.

This conclusion has an immediate consequence for the fractal dimension of the invariant measure generated by an optimal nonperiodic orbit. In particular, the information dimension of an invariant measure of the map (2) has been shown [10] to be the metric entropy divided by ln2; the latter quantity is the Lyapunov exponent of the map (2). Thus optimal nonperiodic orbits also have information dimension zero. Hence these orbits, although nonperiodic, are similar to periodic orbits in that they have zero entropy and zero dimension.

III. THE TENT MAP WITH A SINGLE-HUMPED PERFORMANCE FUNCTION

We consider next the tent map on $[0,1]$,

$$x_{t+1}=\begin{cases}2x_t & x_t\leqslant 1/2\\ 2(1-x_t) & x_t\geqslant 1/2,\end{cases} \tag{5}$$

with the same performance function (3). Results, based again on 10^5 evenly spaced values of γ and orbits of period up to 24, are shown in the second and third columns of Table II and in Fig. 7. We see that, again, most of the time optimization is obtained at low period. (For instance, for more than 87% of the γ values the optimum period is 4 or less; if one is willing to settle for 90% of optimal, one never need go above period 5.) The excellent agreement of the large p data with $f(p)=Kp2^{-p}$ shown in the last column of Table II again implies an overall exponential decrease of the Lebesgue measure corresponding to γ values yielding optimization at period p or greater. The value $K=0.234$ used in this case is derived analytically in Appendix A.

Referring to Fig. 7, we see a structure very different from the Farey structure observed in Fig. 1. In particular, as γ decreases from $\gamma=1$, there is a succession of step increases, starting with period $p=1$, as the optimal period changes from p to $p+1$. Exactly at the γ value γ_p corresponding to the step increase from period p to period $p+1$, the averages $\langle F_\gamma\rangle_p$ and $\langle F_\gamma\rangle_{p+1}$ are equal, and are larger than $\langle F_\gamma\rangle_{p'}$ for all $p'\neq p,p+1$. For γ near γ_p and $\gamma<\gamma_p$ ($\gamma>\gamma_p$) we numerically observe that $\langle F_\gamma\rangle_p>\langle F_\gamma\rangle_{p+1}$ ($\langle F_\gamma\rangle_p>\langle F_\gamma\rangle_{p+1}$). The situation is qualitatively similar to that in the inset to Fig. 3, except that the dotted line, which would correspond in this case to $\langle F_\gamma\rangle_{2p+1}$, lies *below* the weighted average of $\langle F_\gamma\rangle_p$ and $\langle F_\gamma\rangle_{p+1}$. Thus there is no γ interval of period $2p+1$ derived by Farey summation between the period-p and period-$(p+1)$ intervals. On the other hand, we can think of each period-$(p+1)$ interval as being created by Farey summation from the adjacent period-p interval and the large period-1 interval. The structure in this example can thus be likened to a single branch (the leftmost) of the Farey tree discussed in Sec. II. As γ decreases further, there are an infinite number of the step increases described above, accu-

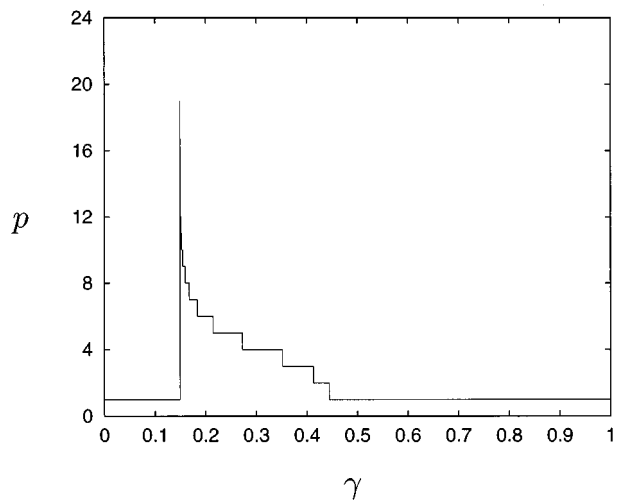

FIG. 7. Period that optimizes $\langle F_\gamma\rangle$ as a function of γ for the tent map (5) and performance function (3).

mulating to the γ value $\gamma_\infty \approx 0.14955$. For $0 < \gamma < \gamma_\infty$ the optimal orbit is the period-1 orbit (fixed point) at $x = 0$.

Again thinking of a nonperiodic orbit as the limit of a sequence of periodic orbits as the period goes to infinity, we infer that the only possible γ value at which optimization might be achieved only by a nonperiodic orbit is $\gamma = \gamma_\infty$. On the other hand, by continuity the interval on which the fixed point $x = 0$ is optimal must be closed, and thus this interval includes γ_∞. We conclude that the set S_γ of γ values for which optimal orbits are nonperiodic is empty in this example.

We remark that many of the conclusions we obtained in this and the previous section ought to be amenable to rigorous analysis of the maps (2) and (5) and the performance function (3). We hope to be able to report such results in a future publication.

Our examples in this section [Eqs. (5) and (3)] and in the previous section [Eqs. (2) and (3)] illustrate two prototypical behaviors, step changes in the optimal period (Fig. 7), and Farey structure (Fig. 1). In the next section we consider several other examples. In all of these examples we find a ''mixture'' of the two types of structure found in this section and in Sec. II. Based on our examples we offer two conjectures concerning typical low-dimensional chaotic systems and typical smooth performance functions with a parameter dependence:

Conjecture 1. The Lebesgue measure of the parameters corresponding to optimal periodic orbits with period p or greater decreases exponentially with p.

Conjecture 2. The set of parameter values for which optimal orbits are nonperiodic has Lebesgue measure zero.

IV. OTHER EXAMPLES

In the remainder of this paper we present some further numerical results involving different choices of the optimization function F and different dynamical systems, in support of the above conjectures and the principle that, for most parameters, $\langle F \rangle$ is maximized by a low-period orbit. The composite Farey-step structure we observe in all these examples is discussed in Sec. IV D.

A. The doubling transformation and the tent map with a multihumped performance function

The fourth column of Table I shows the fraction of 10^5 evenly spaced values of γ for which a period-p orbit of the map (2) maximizes the average of a different function:

$$F_\gamma(x) = \cos[2\pi(x-\gamma)] + \sin[6\pi(x-\gamma)]. \tag{6}$$

The fifth column of Table I gives the corresponding fraction for the lowest p within 90% of optimal. The function in Eq. (6) has three local maxima and three local minima. This increases the likelihood of a higher-period orbit maximizing $\langle F_\gamma \rangle$, as is reflected in the data. The Farey structure, present for smooth functions with a single maximum [e.g., Eq. (3)], is found only partially in this case (and in the examples with two-dimensional maps that follow). Thus the number of intervals $N(p)$ for which a period-p orbit maximizes $\langle F_\gamma \rangle$ is in general not equal to the Euler function $\phi(p)$. However, we find that the size of each period-p interval still tends to scale as $p2^{-p}$; if we replace the Euler functions $\phi(p)$ in Eq. (4) by the numerically observed number of γ intervals $N(p)$ for which a period-p orbit maximizes $\langle F_\gamma \rangle$, good agreement with Eq. (4) is restored. This is illustrated by the data represented as squares in Fig. 2. Another important point is that for Eq. (6) [as for Eq. (3)] we observe an exponential decrease, as a function of p, of the proportion $r(p)$ of phase values γ for which $\langle F_\gamma \rangle$ is maximized on an orbit of period at least p. This is shown by the data plotted as squares in Fig. 5. Thus the result that low-period orbits most often are optimal is apparently independent of our choice of F.

Similar results and conclusions apply for the tent map (5) with the multihumped performance function (6). Data corresponding to this case are given in the fourth and fifth columns of Table II.

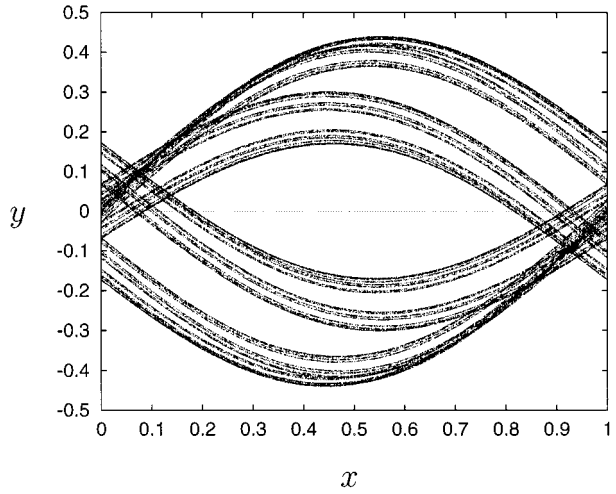

FIG. 8. Attractor for Kaplan-Yorke map with $\lambda = 0.4$.

B. The Kaplan-Yorke map

The above discussion was for a one-dimensional map. How do these results carry over into higher dimensionality? To get some indication of the situation we consider two different two-dimensional maps. First we discuss the Kaplan-Yorke map [11],

$$x_{n+1} = 2x_n \ \ (\text{modulo}1), \tag{7a}$$

$$y_{n+1} = \lambda y_n + \frac{1}{\pi}\sin(2\pi x_n). \tag{7b}$$

The Lyapunov exponents are $\ln 2$ and $\ln\lambda$. Choosing $\lambda = 0.4$ we have an information dimension of $D \approx 1.76$ for the attractor. A picture illustrating the fractal structure of the attractor appears in Fig. 8. Results for the optimal period with F chosen to be

$$F_\gamma(x,y) = \cos[2\pi(x+y-\gamma)] \tag{8}$$

are shown in the second and third columns of Table III, and in Fig. 9. The scaling of the average size of the γ interval on which a given period-p orbit maximizes $\langle F_\gamma \rangle$ is shown by the triangles in Fig. 2, and the decay of the proportion $r(p)$ of γ values for which $\langle F_\gamma \rangle$ is maximized by an orbit of

TABLE III. Numerical results for 2D maps.

	Kaplan-Yorke Map (7, 8)		Hénon Map (9, 10)	
p	$f(p)$	$f_{90\%}(p)$	$f(p)$	$f_{90\%}(p)$
1	0.282	0.319	0.427	0.434
2	0	0	0.421	0.424
3	0	0	0	0
4	0.140	0.188	0.0862	0.0857
5	0.223	0.326	0	0
6	0.127	0.139	0.00823	0.0352
7	0.0768	0.0285	0.0415	0.0210
8	0.0466	0	0	0
9	0.0524	0	0	0
10	0.0162	0	0	0
11	0.0169	0	0	0
12	0.00518	0	0.00915	0
13	0.00750	0	0.00531	0
14	0.00274	0	0	0
15	0.00158	0	0	0
16–24	0.00214	0	0.00205	0

period at least p is depicted by the triangles in Fig. 5. These results offer further support for our conjectures.

C. The Hénon map

Next we consider the Hénon map

$$x_{n+1} = a + by_n - x_n^2, \tag{9a}$$

$$y_{n+1} = x_n, \tag{9b}$$

with the often studied parameter values $a = 1.4$, $b = 0.3$. The periodic orbits of this map were found using the method of [12], and the function we averaged was

$$F_\gamma(x,y) = \cos[(\pi/2)(x + y - \gamma)]. \tag{10}$$

There are many fewer orbits of a given period for this map than in the previous cases, thus orbits of period up to 30 were considered (there are approximately 10^5 such orbits). The results are given in the fourth and fifth columns of Table III, and by the crosses in Figs. 2 and 5. Evidently the principle that the optimum is typically achieved by low-period orbits, and that near optimum performance can always be achieved by such orbits, continues to hold.

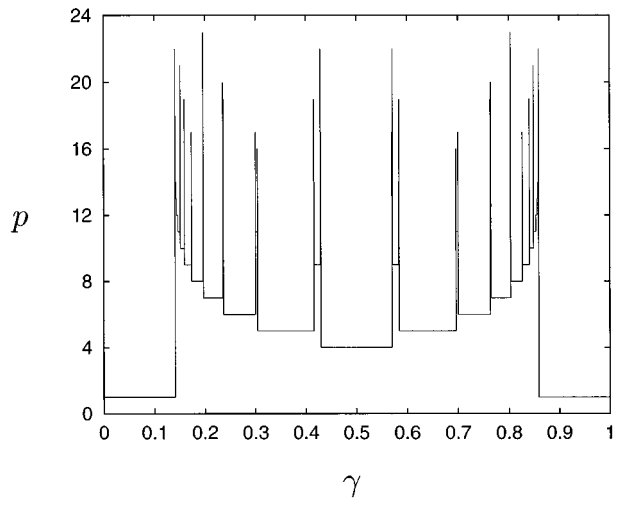

FIG. 9. Period that optimizes $\langle F_\gamma \rangle$ as a function of γ for the Kaplan-Yorke map (7) and performance function (8).

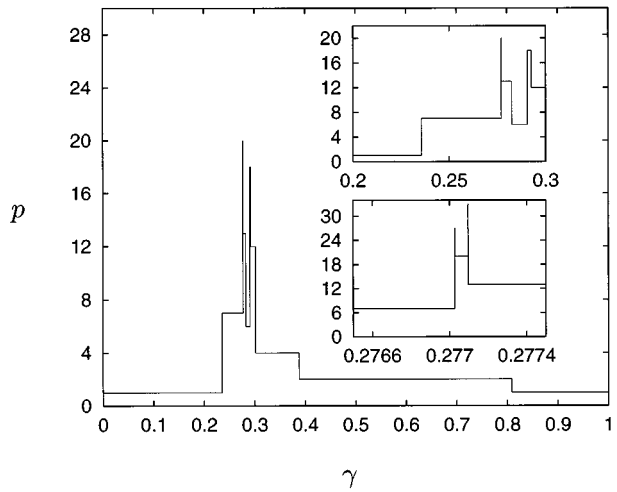

FIG. 10. Period that optimizes $\langle F_\gamma \rangle$ as a function of γ for the Hénon map (9) and performance function (10). Periods 1–30 were considered. Top inset: closeup of region with large periods. Bottom inset: further closeup showing even larger periods detected using γ values spaced 10^{-7} apart and orbits up to period 33.

D. Farey tree structure

Finally, we note that in all the cases we studied in this section, the Farey tree structure we found in the prototype case of Sec. II is still partially present. For example, in Fig. 10 we see the maximizing period as a function of γ for the Hénon map example above. There are ''step'' transitions (as in Sec. III) from period 1 to 2, 2 to 4, and so on; however, in the insets we see that the high-period γ intervals near $\gamma = 0.3$ are created by Farey summation: between the period-1 interval and the period-6 interval there is a period-7 interval, between periods 7 and 6 there is period 13, between 7 and 13 there is period 20, and on either side there are periods 27 and 33; also between period 6 and 12 there is period 18. Similarly in the other cases we see that there can be step transitions between low-period γ intervals, but that when high-period intervals are created they follow the Farey pattern. Since the set S_γ with optimal nonperiodic orbits results from the limit as the period goes to infinity, the occurrence of the higher-period orbits in a Farey sequence suggests that our arguments in the case of Eqs. (2) and (3) that S_γ (if nonempty) is a Cantor set with fractal dimension zero and that optimal nonperiodic orbits have metric entropy zero carry over to the other cases.

V. FURTHER DISCUSSION

In the past, experimentalists working on controlling chaos have often experimentally determined only low-period unstable periodic orbits embedded in the chaotic attractor. This is partly because the determination of many high-period unstable periodic orbits can be very demanding and in many

cases not feasible. Our work in this paper indicates that there will usually be little gain, and often none, by going to the considerable effort of determining many more embedded periodic orbits.

ACKNOWLEDGMENTS

We thank H. Kaplan, A. Lopes, D. Mauldin, M. Rychlik, J. Yorke, and L.-S. Young for helpful discussions. This research [13] was supported by the U.S. Department of Energy (Offices of Scientific Computing and Energy Research), by the National Science Foundation (Divisions of Mathematical and Physical Sciences), and by the Office of Naval Research. The numerical computations reported in this paper were made possible by a grant from the W. M. Keck Foundation.

APPENDIX A

In arriving at Eq. (4) we use the numerical observation that the width in γ of an interval with an optimal period-p orbit scales as $p2^{-p}$ for large p. In this Appendix we derive this result analytically for Eqs. (5) and (3), and indicate how our analysis extends to the case of Eqs. (2) and (3) as well.

Let I_p be the period-p interval depicted in Fig. 7. Numerically we observe that each I_p for $p \geqslant 2$ corresponds to the period-p orbit of the tent map

$$\frac{2}{2^p+1} \to \frac{4}{2^p+1} \to \frac{8}{2^p+1} \to \cdots \to \frac{2^p}{2^p+1} \to \frac{2}{2^p+1} \to \cdots .$$

As in Sec. III, let γ_p be the endpoint in common between I_p and I_{p+1}. Then the width of I_p is equal to $\gamma_{p-1}-\gamma_p$. As we discussed in Sec. III, when $\gamma=\gamma_p$ the averages $\langle F_\gamma \rangle_p$ and $\langle F_\gamma \rangle_{p+1}$ are equal. That is,

$$\frac{1}{p}\sum_{k=1}^{p} F_\gamma\left(\frac{2^k}{2^p+1}\right) = \frac{1}{p+1}\sum_{k=0}^{p} F_\gamma\left(\frac{2^{k+1}}{2^{p+1}+1}\right). \quad \text{(A1)}$$

To estimate the difference between γ_p and the accumulation point γ_∞ of the intervals I_p as $p\to\infty$, we make a series of approximations to the difference between the two sides of Eq. (11), retaining terms of order 2^{-p} but throwing away terms of order 2^{-2p}. Multiplying both sides of Eq. (11) by $p(p+1)$ and subtracting yields

$$\begin{aligned}
0 &= p\sum_{k=0}^{p} F_\gamma\left(\frac{2^{k+1}}{2^{p+1}+1}\right) - (p+1)\sum_{k=1}^{p} F_\gamma\left(\frac{2^k}{2^p+1}\right) \\
&= \sum_{k=1}^{p}\left[F_\gamma\left(\frac{2}{2^{p+1}+1}\right) + pF_\gamma\left(\frac{2^{k+1}}{2^{p+1}+1}\right) - (p+1)F_\gamma\left(\frac{2^k}{2^p+1}\right)\right] \\
&\approx \sum_{k=1}^{p}\{F_\gamma(0)+2^{-p}F'_\gamma(0)+p[F_\gamma(2^{k-p})-2^{k-2p-1}F'_\gamma(2^{k-p})]-(p+1)[F_\gamma(2^{k-p})-2^{k-2p}F'_\gamma(2^{k-p})]\} \\
&= \sum_{k=1}^{p}[F_\gamma(0)-F_\gamma(2^{k-p})+2^{-p}F'_\gamma(0)+(p+2)2^{k-2p-1}F'_\gamma(2^{k-p})].
\end{aligned}$$

Substituting $n=p-k$ we proceed to get

$$\begin{aligned}
0 &\approx \sum_{n=0}^{p-1}[F_\gamma(0)-F_\gamma(2^{-n})+2^{-p}F'_\gamma(0)+(p+2)2^{-p-n-1}F'_\gamma(2^{-n})] \\
&\approx \sum_{n=0}^{\infty}[F_\gamma(0)-F_\gamma(2^{-n})]+\sum_{n=p}^{\infty}2^{-n}F'_\gamma(0)+p2^{-p}F'_\gamma(0)+(p+2)2^{-p-1}\sum_{n=0}^{\infty}2^{-n}F'_\gamma(2^{-n}) \\
&= \sum_{n=0}^{\infty}[F_\gamma(0)-F_\gamma(2^{-n})]+(p+2)2^{-p-1}\sum_{n=0}^{\infty}2^{-n}[F'_\gamma(0)+F'_\gamma(2^{-n})].
\end{aligned}$$

In the limit as $p\to\infty$ the above approximation becomes exact, and thus when $\gamma=\gamma_\infty$,

$$\sum_{n=0}^{\infty}[F_\gamma(0)-F_\gamma(2^{-n})]=0.$$

It follows that

$$\gamma_p-\gamma_\infty \approx -(p+2)2^{-p-1}\left.\frac{\Sigma_{n=0}^{\infty}2^{-n}[F'_\gamma(0)+F'_\gamma(2^{-n})]}{\Sigma_{n=0}^{\infty}[(\partial/\partial\gamma)F_\gamma(0)-(\partial/\partial\gamma)F_\gamma(2^{-n})]}\right|_{\gamma=\gamma_\infty},$$

and consequently that

$$\gamma_{p-1}-\gamma_p \approx Kp2^{-p},$$

where

$$K=\left.\frac{\Sigma_{n=0}^{\infty}2^{-n}[F'_\gamma(0)+F'_\gamma(2^{-n})]}{2\Sigma_{n=0}^{\infty}[(\partial/\partial\gamma)F_\gamma(0)-(\partial/\partial\gamma)F_\gamma(2^{-n})]}\right|_{\gamma=\gamma_\infty}.$$

In the case of Eqs. (5) and (3), we obtain $K\approx 0.234$.

An analogous argument can be made in the case of Eqs. (2) and (3). In Fig. 1 we observe a similar sequence of intervals I_p accumulating to the left toward $\gamma\approx 0.14955$. Though there are higher-period intervals intervening between consecutive I_p, we find the widths of these higher-period intervals to be negligible compared with the widths of the surrounding I_p. Repeating the above analysis yields in this case

$$K=\left.\frac{\Sigma_{n=1}^{\infty}2^{-n}[F'_\gamma(0)-F'_\gamma(2^{-n})]}{2\Sigma_{n=1}^{\infty}[(\partial/\partial\gamma)F_\gamma(0)-(\partial/\partial\gamma)F_\gamma(2^{-n})]}\right|_{\gamma=\gamma_\infty}\approx 0.150.$$

Similar but more complicated formulas can be derived for the values of K corresponding to other steplike cascades of γ intervals in Fig. 1; remarkably, our numerical results indicate that all such values of K are near to 1/6.

APPENDIX B

We consider two periodic orbits of length p_a and p_b, where we take the convention $p_a \geqslant p_b$, and assume the two orbits are encoded symbolically by strings of zeros and ones. We wish to obtain an upper bound on the metric entropy of an orbit that spends all its time tracking one or the other of these orbits, so that its symbolic dynamics can be formed by concatenating successive copies of the symbol strings for the two periodic orbits. This is the situation for optimal orbits of Eqs. (2) and (3) in the Farey tree; see Fig. 6. For large N, we ask how many distinct strings of length N one can form from blocks consisting of the p_a and p_b strings. For simplicity we assume N is an integer multiple of p_a. We divide a string of length N into substrings of length p_a and ask how many ways each substring can be divided into the building blocks of type p_a and p_b. We allow for partial blocks at each end of the substring, and do not worry about these partial blocks matching up from one substring to the next—thus our eventual count of the number of distinct strings of length N will be an overestimate.

The number of possible partitions of a substring of length p_a is bounded above by the number of possibilities for the starting block (or partial block) times the number of possibilities for the ending block (or partial block). This is because the space (if any) between these blocks must be filled with blocks of type p_b. The starting block can be a block of type p_a or a partial block thereof with length $1,2,\ldots,p_a-1$, giving p_a possibilities. Likewise there are p_b possible starting blocks or partial blocks of type p_b, for a total of p_a+p_b possibilities. Similarly there are p_a+p_b possible ending blocks, for a total of, at most, $(p_a+p_b)^2$ possible partitions of a given substring of length p_a.

This analysis gives an upper bound of $(p_a+p_b)^{2N/p_a}$ possible strings of length N when the building blocks have lengths $p_a \geqslant p_b$. The entropy in this situation is thus bounded above by

$$\frac{1}{N}\ln[(p_a+p_b)^{2N/p_a}]=\frac{2}{p_a}\ln(p_a+p_b).$$

Thus, as p_a is allowed to approach infinity, this expression goes to zero, and we conclude that the entropy of a nonperiodic orbit is zero.

[1] E. Ott, C. Grebogi, and James A. Yorke, Phys. Rev. Lett. **64**, 1196 (1990).

[2] J. C. Alexander, I. Kan, J. A. Yorke, and Z. You, Int. J. Bifurc. Chaos **2**, 795 (1992); E. Ott, J. C. Sommerer, J. C. Alexander, I. Kan, and J. A. Yorke, Phys. Rev. Lett. **71**, 4134 (1993); J. C. Sommerer and E. Ott, Nature **365**, 136 (1993).

[3] E. Ott, J. C. Sommerer, J. C. Alexander, I. Kan, and J. A. Yorke, Physica D **76**, 384 (1994).

[4] Another related situation occurs in the ''bubbling transition'' [5,6] first noted by Ashwin *et al.* [5]. This transition is marked by the onset of temporally intermittent bursting in the presence of small noise (see Refs. [3,5] and the paper of N. Platt, S. M. Hammel, and J. F. Heagy, Phys. Rev. Lett. **72**, 3498 (1994)).

[5] P. Ashwin, J. Buescu, and I. Stewart, Phys. Lett. **193A**, 126 (1994).

[6] S. C. Venkataramani *et al.*, Phys. Rev. E (to be published); Y.-C. Lai *et al.*, Phys. Rev. Lett. (to be published).

[7] J. A. Yorke (private communication) has suggested that the bifurcation is typically mediated by a periodic orbit, and this conjecture is supported by this paper.

[8] A different but related result has been obtained by B. R. Hunt and J. A. Yorke, who argue that a certain type of crisis bifurcation of a chaotic attractor is typically mediated by a low period unstable periodic orbit [Trans. Am. Math. Soc. **325**, 141 (1991)].

[9] This line of argument is supported by the work of K. Sigmund, who proved that for hyperbolic systems, every invariant measure can be approximated arbitrarily well by the δ-function measure on a periodic orbit [Am. J. Math. **94**, 31 (1972)].

[10] L.-S. Young, Erg. Th. Dyn. Syst. **2**, 109 (1982).

[11] J. L. Kaplan and J. A. Yorke, in *Functional Differential Equations and Approximation of Fixed Points*, edited by H.-O. Peitgen and H.-O. Walter, Lecture Notes in Mathematics Vol. 730 (Springer, Berlin, 1979), p. 204.

[12] O. Biham and W. Wenzel, Phys. Rev. Lett. **63**, 819 (1989); see also P. Grassberger, H. Kantz, and U. Moenig, J. Phys. A **22**, 5217 (1989).

[13] Some of the results in this paper were reported in abbreviated form in B. R. Hunt and E. Ott, Phys. Rev. Lett. **76**, 2254 (1996).